Regular Article

# The effect of boron on oxide scale formation in a new polycrystalline superalloy

Paraskevas Kontis, Stella Pedrazzini, Yilun Gong, Paul A.J. Bagot, Michael P. Moody, Roger C. Reed *

Department of Materials, University of Oxford, Parks Road, OX1 3PH Oxford, UK

## ABSTRACT

Boron addition to a new polycrystalline nickel-based superalloy promotes the formation of a hitherto unreported aluminoborate phase, in the scale produced by oxidation in air at 900 °C for ~10,000 h. Atom probe tomography provides unambiguous confirmation of this. The ramifications of its formation are discussed.

© 2016 Acta Materialia Inc. Published by Elsevier Ltd. This is an open access article under the CC BY license (http://creativecommons.org/licenses/by/4.0/).

Very little is known about the role played by grain boundary elements such as boron on the oxidation behaviour of the nickel-based superalloys [1,2]. The difficulty in detecting this element – particularly at the necessary spatial resolution – has contributed to this situation. Traditionally, electron microscopy and/or X-ray diffraction have been used for the characterisation of the oxidation reaction in these materials [3]. Consequently, the collection of accurate chemical composition data for boron from oxides is not generally deemed feasible. Peak overlapping issues in the case of certain elements – such as chromium and oxygen – also present difficulties. However, recent improvements in analytical techniques – such as atom probe tomography (APT) – allow in principle more accurate measurements. Atom probe tomography is a 3D characterisation method which provides chemical resolution on the nanoscale. It has great potential to generate invaluable insight into the chemistry of oxides [4–6].

Nevertheless, analysis of brittle, thermally and electrically insulating samples using the APT method is still in itself very challenging. In-depth studies therefore of oxidation behaviour which encompasses 3D distributions of chemical compositions and segregation are rather limited and rare. But recent developments both in instrumentation and sample preparation techniques are now facilitating APT measurements on oxide scales [7,8]. In the present study, a multi-scale investigation was performed using a suite of characterisation techniques to provide an understanding of the oxidation behaviour of a boron-containing polycrystalline superalloy.

A recently developed polycrystalline superalloy suitable for power generation applications was used in this study, known as STAL15-CC

[9], see Table 1. After conventional casting, a hot isostatic press (HIP) – at 1195 °C for 5 h under 175 MPa pressure – was used to consolidate the as-cast bars, to eliminate microporosity and improve mechanical properties. The process of HIP was followed by a stage of primary ageing at 1120 °C for 4 h and a subsequent second stage of ageing at 845 °C for 24 h, both followed by air-cooling. Fully heat-treated specimens of 10 mm × 15 mm × 3 mm thickness were isothermally exposed at 900 °C in air for ~10,000 h.

An overview of the morphology of the oxide – obtained using a Zeiss Merlin field emission gun-scanning electron microscope (FEG-SEM) – is illustrated in the backscattered SEM micrograph of Fig. 1. Careful examination of the scale indicates three different oxide layers; a schematic representation of the oxide scale is given. To provide a first insight into the composition of the oxide layers spot analyses were performed within each layer using a Zeiss Merlin microscope, at 4 keV. The red boxes in Fig. 1(a) indicate areas for energy dispersive X-ray (EDX) spot analysis with the corresponding spectrum shown in Fig. 2(a). The internal layer was found to be Al-rich as illustrated in Fig. 2(a) and it has formed a continuous layer. This is consistent with the data of Sato et al. [10] who investigated previously the oxidation character of the single crystal version of STAL15 – which for the avoidance of doubt is not doped with boron. There, a continuous alumina $Al_2O_3$ layer was confirmed by SEM, X-ray diffraction (XRD) and transmission electron microscopy (TEM) in specimens exposed at 900 °C for 100 h. Thus the formation of the alumina layer is expected in the conventional cast version of STAL15, confirming the strong alumina-forming characteristics of this system.

But in the boron-doped STAL15-CC considered here the intermediate oxide is enriched in boron, see Fig. 2(b); its Al content is less than in the alumina below it. Note that the Cr content cannot be evaluated

* Corresponding author.
E-mail address: roger.reed@eng.ox.ac.uk (R.C. Reed).

**Table 1**
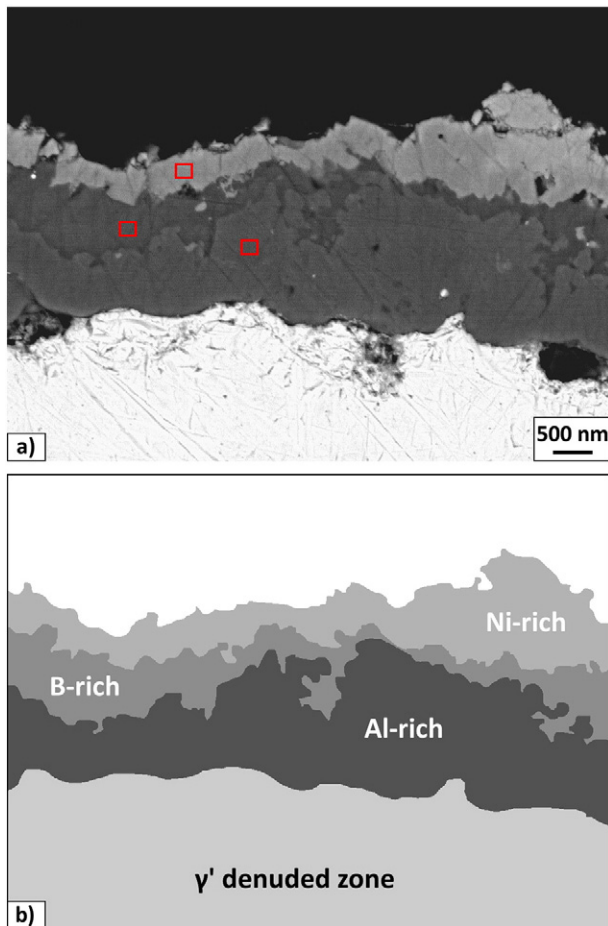Chemical composition of the STAL15-CC investigated in this work (at.%).

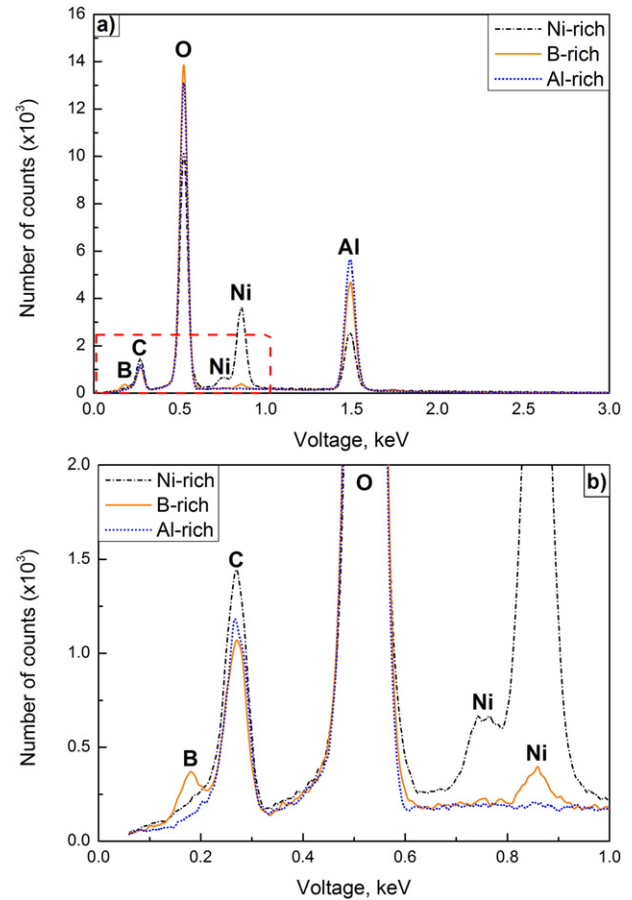| B | C | Co | Cr | Mo | W | Al | Ta | Hf |
|---|---|---|---|---|---|---|---|---|
| 0.05 | 0.47 | 5.50 | 16.55 | 0.59 | 1.26 | 10.09 | 2.40 | 0.02 |

due to overlapping between the oxygen and chromium peaks at such low keV EDX levels. The outer oxide was found to be enriched in nickel, whereas the aluminium content is decreased still further. Within the detection limits of the EDX method, there was no indication of boron being incorporated in the outer oxide.

Atom probe tomography circumvents the challenges associated with the EDX method and thus provides quantitative information concerning the compositions of the intermediate and outer oxide. Site specific lift-outs were prepared for atom probe tomography from the boron and nickel-rich oxides, using procedures described in Ref. [11]. Samples were analysed using a Cameca LEAP 5000 XR instrument operating in laser mode with pulse rate at 100 kHz, pulse energy 50 pJ and temperature 50 K.

The compositions measured by APT for the boron and nickel-rich oxides are given in Table 2. The outer oxide corresponds to a spinel phase with a stoichiometry of $Ni(Al,Cr)_2O_4$. In the case of the intermediate oxide, the stoichiometry corresponds to $Al_4B_2O_9$ [12]; this aluminoborate phase has not been reported before in oxidised nickel-based superalloys. Recently a different boron oxide with a stoichiometry



**Fig. 2.** a) Point EDX analysis corresponding to the oxide areas denoted by the red boxes in Fig. 1(a) and b) detail of the part of the EDX spectrum as denoted by the red dashed box.



**Fig. 1.** Specimen from the boron-containing STAL15-CC alloy exposed isothermally at 900 °C for ~10,000 h: a) backscattered SEM micrograph of the oxide scale and b) corresponding schematic representation of the oxide scale. The red boxes denote the areas of point EDX analysis (see data in Fig. 2).

of $BCrO_3$ was observed in the polycrystalline nickel-based Rene 80 after exposure at 1050 °C resulting in substantial boron depletion after 100 h; such type of oxide was not observed in the current study [13].

The formation of the oxides observed in the current study has been rationalised using thermodynamic calculations, see Fig. 3. The possibility for formation of all major oxide and metallic phases was accounted for in the calculations, which were carried out using the Thermo-Calc software coupled with the TCNI8 and SSUB5 thermodynamic databases [14]. The oxygen activity (content) in the system was controlled by replacing the nickel (for the outer spinel layer) or the nickel and chromium (with atomic ratio of 2:1) for the inner layer where chromium depletion due to outward growth nature of Cr-rich spinel can occur (oxygen activity at the $Al_4B_2O_9$ & spinel interface is calculated to be approximately $10^{-10}$). Note that the amount of $Cr_2O_3$ predicted (short-dot line in Fig. 3) depends on such depletion which has a time-dependent character. Therefore, the evaluation of $Cr_2O_3$ formation at the oxide scale needs to be investigated at shorter exposure times. An aluminoborate phase ($Al_4B_2O_9$) is clearly predicted by the thermodynamic calculations which is stable between the internal $Al_2O_3$ layer and the outer spinel scale. The formation of the aluminoborate phase would require the

**Table 2**
Chemical composition of the oxides as measured by APT (at.%).

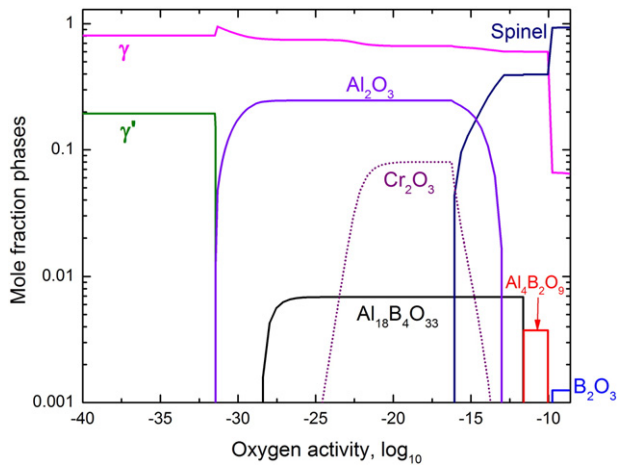| | Al | B | Cr | Ni | Si | O |
|---|---|---|---|---|---|---|
| $Al_4B_2O_9$ | 25.0 | 12.1 | 2.2 | 0.1 | 0.4 | 60.0 |
| $Ni(Al,Cr)_2O_4$ | 5.7 | – | 27.2 | 10.1 | 0.1 | 56.9 |

**Fig. 3.** Thermodynamic calculations at 900 °C predicting the stability of oxide phases for the investigated boron-containing STAL15-CC alloy. Note that the left of the graph corresponds to metallic bulk.

diffusion of boron through the $Al_2O_3$ layer. However, further APT analysis focusing on the internal $Al_2O_3$ layer is required.

The aluminoborate phase contains considerably high amounts of boron thus it is likely to result in substantial boron depletion from the grain boundaries where in the bulk it prefers to reside. As a consequence the mechanical properties will be altered. It has been shown that in the absence of boron from the grain boundaries the creep performance and ductility of STAL15-CC were very poor resulting in very early fracture at elevated temperatures [9].

Different factors are likely to influence the diffusion of boron towards the oxide scale, for example temperature and grain size. In addition, the state in which boron resides at grain boundaries will play an important role. In particular, in STAL15-CC boron was found to form intergranular Cr-rich $M_5B_3$ borides rather than being in solid solution after full heat treatment was applied [9]. By contrast, in many other superalloys boron was found in solid solution along the grain boundaries [15, 16]. In that case, the diffusion of boron towards the oxide scale will be faster; thus boron depletion from the microstructure will occur in shorter exposure times. A comparison of the diffusion rate of boron accounting for different states in which it resides at grain boundaries was calculated previously for the polycrystalline nickel-based Rene 80, showing that partitioning of boron into $M_3B_2$-type borides results in slower boron depletion [13].

It is therefore suggested that boron in the form of borides is more preferable than in solution at the grain boundaries. However, attention needs to be given to the boron content and thus the volume fraction of borides; above a certain boron threshold borides can be detrimental rather than beneficial to the mechanical properties [17]. It becomes apparent that the addition of grain boundary elements required for the design of new polycrystalline superalloys needs to be carefully selected.

An APT 3D reconstruction from the aluminoborate phase is illustrated in Fig. 4(a); grain boundaries are highlighted by segregation of Si. A 1D concentration profile across a grain boundary as indicated by the cylindrical region of interest in Fig. 4(a) is shown in Fig. 4(b).

Co-segregation of Si, B and Ni at the grain boundaries of the aluminoborate phase is clearly observed. Silicon was found to have a beneficial effect on the oxidation resistance by promoting the formation of a continuous alumina layer in the nickel-based single-crystal superalloy STAL15 – previously known as SCA425+ [10]. Similarly, although it has been suggested that Si segregates at the grain boundary of alumina, no clear evidence of this has been presented so far [18]. Here, the segregation of Si at the grain boundaries of the aluminoborate phase was confirmed by the APT analysis as shown in Fig. 4(b).

Analysis of grain boundary chemistry in the aluminoborate phase proved possible with APT, with boron segregation confirmed. The
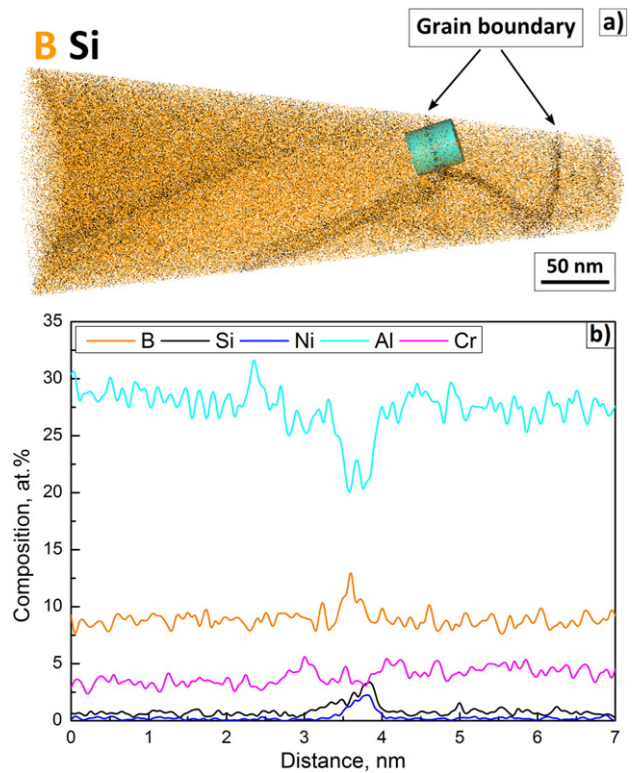


**Fig. 4.** a) An atom probe 3D reconstruction from the boron-rich oxide with grain boundaries highlighted with Si and b) corresponding 1D concentration profile from the cylindrical region of interest across a grain boundary.

accumulation of boron at the inner oxide of a novel γ/γ′ Co-based superalloy has been suggested to improve the oxide layer adhesion [19]. In a similar way, the segregation of boron at the grain boundaries of the aluminoborate phase will potentially result in improved oxide layer adhesion, but further studies are needed to confirm this conjecture.

To summarise, although the use of boron as a grain boundary strengthener in the nickel-based superalloys is well accepted, its effect on oxide scale formation is new. In this study, an aluminoborate phase is reported in this system for the first time. Its chemistry and composition have been confirmed unambiguously by APT analysis; it corresponds to $Al_4B_2O_9$. A recently developed polycrystalline superalloy exposed isothermally in air for ~10,000 h at 900 °C was used, of the grade which will likely enter commercial service soon. It is becoming apparent that the depletion of boron from the microstructure can substantially limit the service life of polycrystalline superalloys by weakening their grain boundaries. Thus, the diffusion of boron towards the oxide scale demands particular attention and further investigation.

### Acknowledgements

### References

[1] R.C. Reed, C.M.F. Rae, in: D.E. Laughlin, K. Hono (Eds.), Physical Metallurgy (Fifth Edition), 5th ed.Elsevier, Oxford 2014, pp. 2215–2290.
[2] N. Birks, G.H. Meier, F.S. Pettit, Introduction to the High Temperature Oxidation of Metals, 2nd ed. Cambridge University Press, 2009.
[3] H.S. Kitaguchi, H.Y. Li, H.E. Evans, R.G. Ding, I.P. Jones, G. Baxter, P. Bowen, Acta Mater. 61 (2013) 1968–1981.

[4]  D.J. Young, T.D. Nguyen, P. Felfer, J. Zhang, J.M. Cairney, Scr. Mater. 77 (2014) 29–32.
[5]  H.S. Kitaguchi, M.P. Moody, H.Y. Li, H.E. Evans, M.C. Hardy, S. Lozano-Perez, Scr. Mater. 97 (2015) 41–44.
[6]  L. Viskari, M. Hörnqvist, K.L. Moore, Y. Cao, K. Stiller, Acta Mater. 61 (2013) 3630–3639.
[7]  S. Pedrazzini, D.J. Child, G. West, S.S. Doak, M.C. Hardy, M.P. Moody, P.A.J. Bagot, Scr. Mater. 113 (2016) 51–54.
[8]  A.L. Fontaine, H.-W. Yen, P.J. Felfer, S.P. Ringer, J.M. Cairney, Scr. Mater. 99 (2015) 1–4.
[9]  P. Kontis, H.A. Mohd Yusof, S. Pedrazzini, M. Danaie, K.L. Moore, P.A.J. Bagot, M.P. Moody, C.R.M. Grovenor, R.C. Reed, Acta Mater. 103 (2016) 688–699.
[10]  A. Sato, Y.-L. Chiu, R.C. Reed, Acta Mater. 59 (2011) 225–240.
[11]  K. Thompson, D. Lawrence, D.J. Larson, J.D. Olson, T.F. Kelly, B. Gorman, Ultramicroscopy 107 (2007) 131–139.
[12]  S.A. Decterov, V. Swamy, I.-H. Jung, Int. J. Mater. Res. 98 (2007) 987–994.
[13]  A. Jalowicka, W. Nowak, D.J. Young, V. Nischwitz, D. Naumenko, W.J. Quadakkers, Oxid. Met. 83 (2015) 393–413.
[14]  Thermo-Calc Software AB, Stockholm, Thermo-Calc 2015b, 2016.
[15]  D. Lemarchand, E. Cadel, S. Chambreland, D. Blavette, Philosophical Mag. A 82 (2002) 1651–1669.
[16]  D. Tytko, P.-P. Choi, J. Klöwer, A. Kostka, G. Inden, D. Raabe, Acta Mater. 60 (2012) 1731–1740.
[17]  B.C. Yan, J. Zhang, L.H. Lou, Mater. Sci. Eng. A 474 (2008) 39–47.
[18]  A. Sato, Y.-L. Chiu, E.A. Marquis, R.C. Reed, Mater. High Temp. 29 (2012) 272–278.
[19]  L. Klein, Y. Shen, M.S. Killian, S. Virtanen, Corros. Sci. 53 (2011) 2713–2720.